Aerospace Science and Technology ••• (••••) •••–•••

Contents lists available at ScienceDirect

Aerospace Science and Technology

www.elsevier.com/locate/aescte

Optimal air route flight conflict resolution based on receding horizon control

Tang Xin-Min [a,b,*], Chen Ping [b], Li Bo [a]

[a] Civil Aviation College of Nanjing University of Aeronautics and Astronautics, Nanjing, 210016, China
[b] The 28th Research Institute of China Electronic Technology Group Corporation, Nanjing, 210007, China

ARTICLE INFO

Article history:
Received 8 October 2015
Received in revised form 21 December 2015
Accepted 22 December 2015
Available online xxxx

Keywords:
Conflict resolution
Next generation air traffic control automation system
Parameter identification
Receding horizon control

ABSTRACT

To deal with the air route flight conflicts caused by abnormal situations during four-dimensional based air traffic operation, the air route flight conflict resolution problem for two aircrafts was addressed. Based on the optimized static single heading angle or ground speed adjustment strategy, we proposed an optimized dynamic mixed conflict resolution strategy based on Receding Horizon Control (RHC), which considered the possibility of one aircraft's ground speed variation. In particular, the wind speed vector disturbance during conflict resolution might lead to a model mismatch, so the maximum likelihood estimation method and the Newton–Raphson iterative algorithm were employed to identify the wind speed vector using the aircraft true airspeed inputs and ground based trajectory measurements. Moreover, we considered the convergence of conflict resolution method based on RHC and proposed the pre-condition that local and global optimization resolution can be achieved. We compared three situations, i.e., static single strategy optimization, dynamic mixed strategy optimization using RHC with one aircraft's ground speed variation, and dynamic mixed strategy optimization using RHC with the wind speed vector disturbance. We demonstrated that the dynamic mixed strategy responds to one aircraft's ground speed disturbance quickly, and resolved conflict by track angle and ground speed adjustments in an effective manner after the wind speed vector being identified accurately.

1. Introduction

Four-dimensional (4D) trajectory operation is an effective strategy for reducing aircraft spacing to facilitate the implementation of high density airspace in the future. Both Next Generation Air Transportation System (NGATS) and Single European Sky Air traffic Management Research (SESAR) employ 4D trajectory based air traffic operation as the core mechanism. However, even if aircraft are equipped with conflict-free 4D trajectories before flight, it is inevitable that they will fail to execute exact the conflict-free 4D trajectories due to disturbances caused by meteorological conditions or various types of emergencies. Therefore, it is necessary to conduct real-time conflict detection and optimal conflict resolution to avoid flight conflict, thereby ensuring the safety and smooth of air traffic operation.

The most recent studies on conflict resolution can be categorized into four areas. First, according to the type of decision maker, they can be divided into centralized or distributed decision making, where the former focuses mainly on the conflict resolution for multiple aircraft from the perspective of ground air traffic control system [1], whereas the latter focuses on conflict resolution from the perspective of the onboard aircraft [2,3]. Furthermore, from the perspective of constraints on of trajectory resolution, these approaches can be divided into free flight and air route flight conditions, where the former only considers aircraft performance constraints, so airspace and air route constraints are not considered [4,6], whereas the latter considers both types of constraints together [7,8]. In addition, depending on the optimization model and method employed, these approaches can be divided into continuous optimization and mixed methods. Continuous optimization methods plan an optimal flight trajectory to facilitate conflict avoidance based on optimal control theory [9,10]. The hybrid optimization method requires optimization of two areas, i.e., the discrete decision variables and the continuous resolution variables [11–16]. Finally, the process of conflict resolution optimization can be divided into static and dynamic optimization, where the former only provides a constant and feasible resolution strategy [17], whereas the latter requires the real-time computation of resolution strategy according to the state of the aircraft until the conflict is resolved [18]. In the expectable future, air traffic

* Corresponding author at: Civil Aviation College of Nanjing University of Aeronautics and Astronautics, Nanjing, 210016, China. Tel.: +8613813952160.
E-mail address: tangxinmin@nuaa.edu.cn (X.-M. Tang).

http://dx.doi.org/10.1016/j.ast.2015.12.024
1270-9638/

Nomenclature

v_{TAS}	true airspeed
v_{GS}	ground speed
φ	heading angle
θ	track angle
ω	drift angle
x	horizontal coordination in the ground inertial reference frame
y	vertical coordination in the ground inertial reference frame
z	flight level of aircraft
$\boldsymbol{x}$	position of aircraft
$\boldsymbol{x}_r$	relative orientation vector of aircraft b to aircraft a
$d_{\min}$	minimal horizontal separation of two aircrafts
$\dot{\boldsymbol{x}}$	ground speed vector
$\dot{x}$	horizontal component of ground speed
$\dot{y}$	vertical component of ground speed
α	crossing angle between the relative speed vector and the motion direction of aircraft a
β	crossing angle between the relative orientation vector and the motion direction of aircraft a
$\Delta\theta_b$	track angle adjustment of aircraft b
$\Delta v_{GS,b}$	ground speed adjustment of aircraft b
$\Delta v^*_{GS,b}$	the optimal ground speed adjustment of aircraft b
$\Delta\theta^*_b$	the optimal track angle adjustment of aircraft b
a_b	acceleration of aircraft b
$\Delta\Gamma$	receding horizon
$\boldsymbol{w}$	wind speed vector
w_1	the first component of wind speed vector
w_2	the second component of wind speed vector
$\Delta\boldsymbol{w}(p_i)$	wind speed forecast error at p_i
$\hat{\boldsymbol{w}}$	maximum likelihood estimation of the wind speed vector
$\boldsymbol{e}_w$	identification error of wind speed vector
$r(p_i, p_j)$	covariance of wind speed error between p_i and p_j
$\boldsymbol{z}_b(k)$	discrete trajectory measurement vector
$\hat{\boldsymbol{z}}_b(k)$	discrete trajectory measurement vector after smoothing
$\Delta\tau$	sampling interval of aircraft position
$\boldsymbol{\lambda}$	position measurement error of aircraft b
$\boldsymbol{R}$	covariance matrix of position measurement error
$\varphi^*_b(k)$	the optimal aircraft heading angle of aircraft b
$v^*_{TAS,b}(k)$	the optimal aircraft true airspeed of aircraft b

operations will still only be allowed on the fix air route, where the aircraft state is still obtained by discrete sampling mechanism such as secondary surveillance radar (SSR) or automatic dependent surveillance-broadcast (ADS-B), while air traffic management will still employ a ground based centralized control automation system. Therefore, centralized and dynamic conflict resolution for a fix air route seems to be more beneficial for the future air traffic management.

In related research into dynamic ground conflict resolution includes, Bousson proposed a conflict resolution method based on model predictive control (MPC), which allows the real-time computation of speed and heading for each aircraft to generated conflict-free trajectories along the predetermined waypoint [19]. Roussos et al. studied collision avoidance under wind uncertainty using MPC and decentralized navigation functions [20]. Chaloulos et al. proposed a hierarchical control structure for air traffic management, which allows medium-term conflict resolution using MPC when combined with aircraft dynamics constraints [21]. Rey proposed a receding horizon loop to deal with the uncertainty on aircraft positions, and a Mixed Integer Linear Program problem was then solved for all the potential conflicts detected within the time windows [22]. Peyronne presented a practical method to solve tactical conflicts and model trajectories to avoid conflicts with B-splines on the considered time horizon [23]. These studies assumed that the wind field could be acquired from meteorological forecast, however, the performance of conflict resolution is clearly affected by the wind field uncertainty. Thus, Mondoloni developed a statistical model of wind prediction uncertainty and analyzed the impact of wind prediction uncertainty on the accuracy of aircraft trajectory prediction [24]. Chaloulos et al. proposed a correlation model for simulating the difference between the actual wind and the meteorological wind forecasts to analyze the impact of wind correction on the probability of conflicts [25]. Matsuno et al. proposed a stochastic optimal control method for determining three-dimensional conflict-free aircraft trajectories under wind uncertainty [26]. Delahaye et al. proposed a wind estimation method using a Kalman filter based on radar tracking provided that onboard true airspeed measures are available, but the observability analysis showed that wind could be estimated only if the trajectories included one or two turns in a given area [27].

According to these studies on dynamic ground conflict resolution method, the wind speed vector variation during conflict resolution might lead to mismatch of predictive model, and estimating the actual wind speed vector in the area of conflict is an issue that affects performance of dynamic conflict resolution. In addition, whether one can get some theoretical guarantees on the convergence haven't been considered yet, and local optimization within a short time horizon may result in failure of resolving potential and global conflicts. In this work, we employed parameter identification to estimate the wind speed vector using the aircraft true airspeed input and ground based trajectory measurements to avoid the failure of conflict resolution caused by wind uncertainty on the accuracy of aircraft trajectory during dynamic conflict resolution. Moreover, we considered the convergence of conflict resolution method based on receding horizon optimization and proposed the pre-condition that the local and global optimization resolution can be achieved.

The remainder of this paper is organized as follows. In Section 2, we describe a horizontal flight conflict detection model based on relative motion before discussing a static single optimal resolution strategy. In Section 3, we propose an optimal dynamic mixed conflict resolution strategy based on receding horizon control (RHC) and a real-time parameter identification method is used to identify wind speed vector, we considered the convergence of conflict resolution method based on RHC and proposed the pre-condition that local and global optimization resolution can be achieved. In Section 4, we consider some cases to verify the performance of conflict resolution based on RHC with an uncertain wind speed vector.

2. Static conflict resolution strategy without disturbance

2.1. Aircraft conflict detection model

In this study, we focus mainly on conflict resolution, so the aircraft can be treated as a mass point and its attitude can be neglected. Let true airspeed and ground speed be v_{TAS} and v_{GS}, respectively, and let heading angle and track angle be φ and θ respectively, if drift angle is small enough and can be ignored, then

Please cite this article in press as: X.-M. Tang et al., Optimal air route flight conflict resolution based on receding horizon control, Aerosp. Sci. Technol. (2016), http://dx.doi.org/10.1016/j.ast.2015.12.024

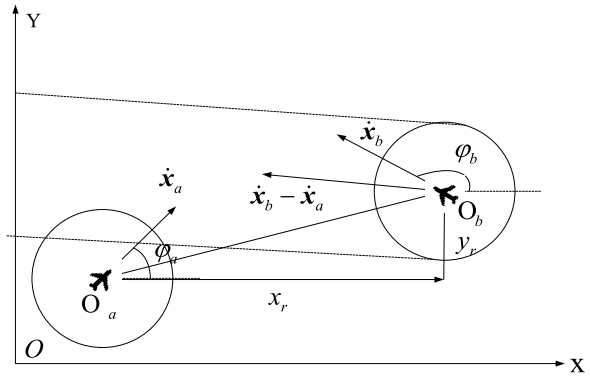

Fig. 1. Relative orientation between two aircrafts.

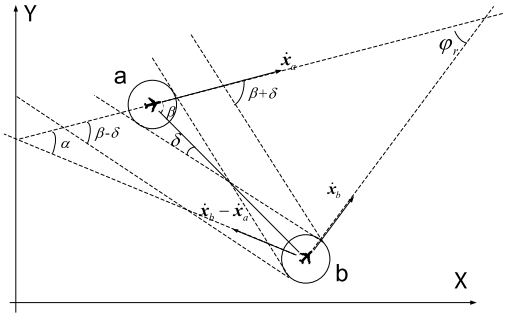

Fig. 2. Detection of potential conflict between two aircrafts.

$\varphi \approx \theta$, and the kinematics equation in the ground inertial reference frame is as follows:

$$\begin{cases} \dot{x} = v_{\mathrm{TAS}} \cos\varphi + w_1 = v_{\mathrm{GS}} \cos\theta \approx v_{\mathrm{GS}} \cos\varphi \\ \dot{y} = v_{\mathrm{TAS}} \sin\varphi + w_2 = v_{\mathrm{GS}} \sin\theta \approx v_{\mathrm{GS}} \sin\varphi. \end{cases} \tag{1}$$

As shown in Fig. 1, let the initial position of aircraft a be $\boldsymbol{x}_a(0) = [x_a, y_a, \varphi_a]^{\mathrm{T}}$ and its ground speed vector be $\dot{\boldsymbol{x}}_a = [v_{\mathrm{GS},a} \cos\varphi_a, v_{\mathrm{GS},a} \sin\varphi_a]^{\mathrm{T}}$, let the initial position of aircraft b be $\boldsymbol{x}_b(0) = [x_b, y_b, \varphi_b]^{\mathrm{T}}$ and its ground speed vector be $\dot{\boldsymbol{x}}_b = [v_{\mathrm{GS},b} \cos\varphi_b, v_{\mathrm{GS},b} \sin\varphi_b]^{\mathrm{T}}$.

In the ground inertial reference frame, the relative orientation of aircraft b to aircraft a can be expressed as

$$\begin{cases} \boldsymbol{x}_r = \begin{bmatrix} x_b - x_a \\ y_b - y_a \end{bmatrix} \\ \varphi_r = \varphi_b - \varphi_a. \end{cases} \tag{2}$$

Let the minimal horizontal separation of the aircraft be $d_{\min}$, then we can determine whether there is a conflict between two aircrafts in the ground inertial reference frame by:

$$\Delta = \|\boldsymbol{x}_r\| - d_{\min}. \tag{3}$$

If $\Delta > 0$, this indicates that there is no conflict between the two aircrafts, otherwise, if $\Delta \le 0$, this indicates that there is conflict between the two aircrafts.

In order to determine the future trend of conflict according to the current position of the aircraft, the relative motion method can be employed. Given the minimal horizontal separation $d_{\min}$, then the protection zone of each aircraft can be defined as a circle with a radius of $R = d_{\min}/2$. The area within two straight lines parallel to $\dot{\boldsymbol{x}}_b - \dot{\boldsymbol{x}}_a$ and tangential to the circle as shown in Fig. 2, is defined as the shadow of aircraft b relative to aircraft a. If the protection zone of aircraft a intersects with the shadow of aircraft b, this indicates that there is potential flight conflict.

In the ground inertial reference frame, we define $\beta = |\varphi_a - \tan^{-1}(y_r/x_r)|$ as the crossing angle between the relative orientation and the motion direction of aircraft a, and we define α as the crossing angle between the relative speed vector and the motion direction of aircraft a,

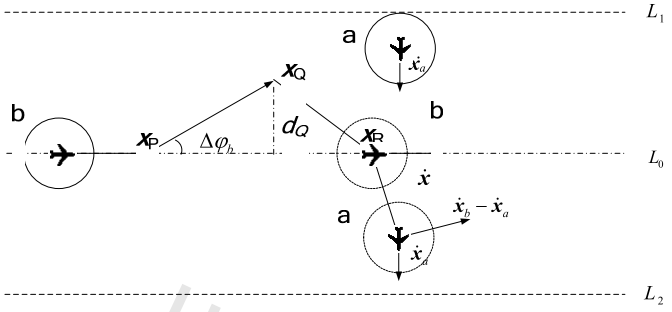

Fig. 3. Trajectory of aircraft b based on heading angle adjustment.

$$\alpha = \tan^{-1}\left| \frac{v_{\mathrm{GS},b} \cdot \sin\varphi_r}{v_{\mathrm{GS},b} \cdot \cos\varphi_r - v_{\mathrm{GS},a}} \right|. \tag{4}$$

Apparently, when α is more than $\beta + \delta$ or less than $\beta - \delta$, the protection zone of aircraft a does not intersect with the shadow of aircraft b, and thus there is no potential conflict. According to the geometrical relationship,

$$\delta = \sin^{-1}\left(\frac{d_{\min}}{\|\boldsymbol{x}_r\|}\right), \tag{5}$$

therefore, the condition for potential conflict avoidance can be given by

$$|\alpha - \beta| \ge \delta. \tag{6}$$

2.2. Conflict resolution based on heading angle adjustment

First, we consider conflict resolution based on heading angle adjustment on the fixed air route. We assume that the ground speed of the two aircrafts remains constant during conflict resolution and that the conflict is resolved only by a heading angle adjustment $\Delta\varphi_b$ of aircraft b.

As shown in Fig. 3, when aircraft b reaches position $\boldsymbol{x}_P$, the resolution procedure begins, and thus α can be obtained as:

$$\alpha = \tan^{-1}\left| \frac{v_{\mathrm{GS},b} \cdot \sin(\varphi_r + \Delta\varphi_b)}{v_{\mathrm{GS},b} \cdot \cos(\varphi_r + \Delta\varphi_b) - v_{\mathrm{GS},a}} \right|. \tag{7}$$

The trajectory of aircraft b on the fixed air route before and after conflict resolutions are shown in Fig. 3, where the two dashed lines L_1 and L_2 denote the air route boundary. Let the air route centerline in the ground inertial reference frame be $L_0 : \boldsymbol{l}_b \cdot \boldsymbol{x}_b = c_b, \boldsymbol{l}_b = [l_1, l_2]$, and let the air route width be $2w$.

After reaching position $\boldsymbol{x}_Q$, aircraft b returns to the air route center using the heading angle adjustment $-\Delta\varphi_b$. Let the distance from $\boldsymbol{x}_Q$ to the air route center be d_Q and the following inequalities then must be satisfied,

$$\begin{cases} d_Q \le w \\ |\alpha_Q - \beta_Q| \ge \delta_Q. \end{cases} \tag{8}$$

If aircraft b reaches position $\boldsymbol{x}_R$ and the inner product of the relative orientation and the relative ground speed vector of two aircrafts is more than zero, then the separation between two aircrafts will continue to increase for the relative motion. In addition, if there is no intersection between the protection zones of the two aircrafts at present, then conflict resolution is completed. Thus, the constraints for the ending position $\boldsymbol{x}_R$ of conflict resolution are:

$$\begin{cases} \boldsymbol{l}_b \cdot \boldsymbol{x}_R - c_b = 0 \\ \boldsymbol{x}_r \cdot (\dot{\boldsymbol{x}}_b - \dot{\boldsymbol{x}}_a) \ge 0 \\ \|\boldsymbol{x}_r\| - d_{\min} > 0. \end{cases} \tag{9}$$

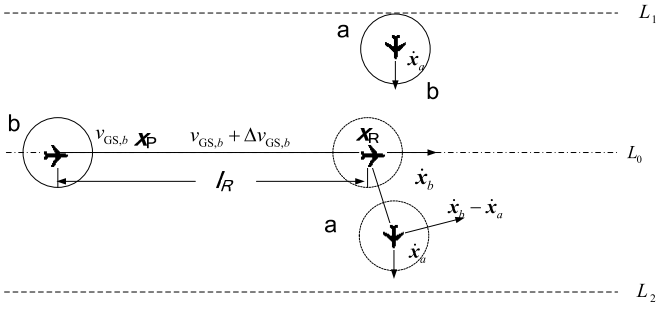

Fig. 4. Trajectories of aircraft b based on ground speed adjustment.

If the duration required to change heading angle of aircraft b is ignored, then the duration of the conflict resolution can be expressed as follows:

$$\Gamma_1 = \frac{2d_Q}{v_{GS,b} \cdot \sin \Delta\varphi_b}. \tag{10}$$

According to the previous analysis, given the initial position of the two aircrafts and the air route boundary constraints, the heading angle adjustment $\Delta\varphi_b$ of aircraft b and the deviation Δd_b from the air route center can be obtained by minimizing the duration of conflict resolution.

2.3. Conflict resolution based on ground speed adjustment

From Eq. (4), it can be inferred that flight conflicts can also be resolved by ground speed adjustment of aircraft b. It is assumed that the heading angle of two aircrafts remains constant during conflict resolution, and the ground speed adjustment of aircraft b is defined as $\Delta v_{GS,b}$, and thus α can be calculated as

$$\alpha = \tan^{-1}\left|\frac{(v_{GS,b}+\Delta v_{GS,b})\cdot \sin\varphi_r}{(v_{GS,b}+\Delta v_{GS,b})\cdot \cos\varphi_r - v_{GS,a}}\right|. \tag{11}$$

Then resolution procedure begins when aircraft b reaches position $\boldsymbol{x}_P$ and the condition for flight conflict avoidance is still as Eq. (6). It is assumed that the aircraft ground speed $\Delta v_{GS,b}$ is only allowed to be within the performance permission interval, i.e., $(v_{GS,b}+\Delta v_{GS,b}) \in [v_{\min,b}, v_{\max,b}]$.

After reaching position $\boldsymbol{x}_Q$, the ground speed of aircraft b returns to the initial ground speed by adjustment $-\Delta v_{GS,b}$, as shown in Fig. 4. When aircraft b reaches position $\boldsymbol{x}_R$ and its ground speed returns to $v_{GS,b}$, the distance between $\boldsymbol{x}_R$ and $\boldsymbol{x}_P$ is assumed to be l_R. The constraints for the ending position $\boldsymbol{x}_R$ of conflict resolution are still Eq. (9).

The duration required to adjusting the ground speed of aircraft b is $2\Delta v_{GS,b}/a_b$, where a_b represents its acceleration, the duration for remaining ground speed $v_{GS,b}+\Delta v_{GS,b}$ is $[l_R - |(v_{GS,b}+\Delta v_{GS,b})^2 - v_{GS,b}^2|/a_b]/(v_{GS,b}+\Delta v_{GS,b})$. Thus the duration of conflict resolution can be expressed as follows:

$$\Gamma_2 = \left\{2\Delta v_{GS,b}\cdot(v_{GS,b}+\Delta v_{GS,b}) + a_b \cdot l_R - |(v_{GS,b}+\Delta v_{GS,b})^2 - v_{GS,b}^2|\right\}\left\{a_b\cdot(v_{GS,b}+\Delta v_{GS,b})\right\}^{-1}. \tag{12}$$

Given the initial position of the two aircrafts and the aircraft performance limit, the ground speed adjustment $\Delta v_{GS,b}$ of aircraft b and the flight distance l_R can be obtained by minimizing the duration of conflict resolution.

3. Dynamic conflict resolution strategy with disturbance

3.1. Conflict resolution optimization based on RHC

In some cases, conflict resolution may be affected by emergency situations or unexpected factors, such as disturbances of the wind speed and variation in the aircraft ground speed, therefore, so conflicts might not be resolved completely using only a static resolution strategy. Receding Horizon Control (RHC) is an optimizing control algorithm within limited time domain, where the future state of the controlled plant could be predicted using the prediction model and optimized in receding horizons [21]. Fig. 5 presents a schematic diagram of RHC, where the computed resolution strategy is only applied when the state is updated again. RHC comprises three basic elements: (1) trajectory and conflict prediction model; (2) resolution optimization in receding horizons; and (3) a correction for prediction model based on wind speed vector identification.

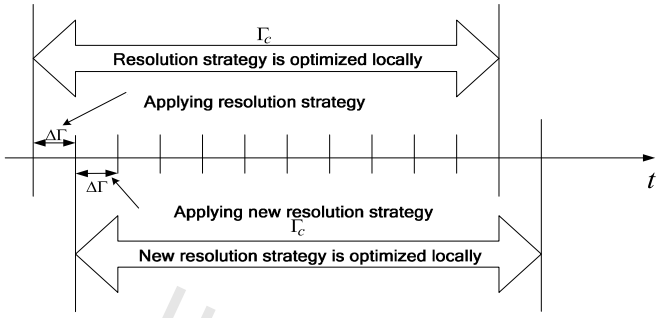

Fig. 5. Schematic diagram of receding horizon control.

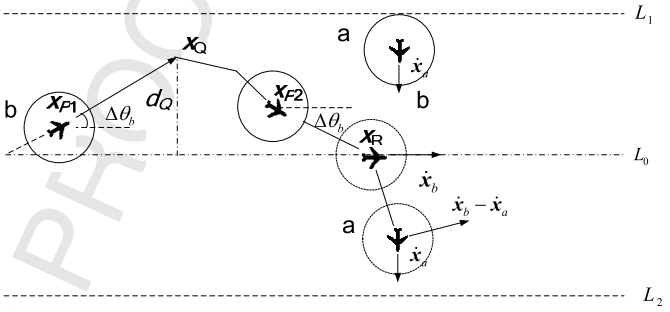

Fig. 6. Trajectories of aircraft b using two control variants.

When optimizing the conflict resolution strategy using RHC, the first step is to establish a conflict resolution model with a predictive function where the assumptions of the model are: (1) the receding horizon is $\Delta\Gamma$; (2) conflict can be resolved based on both track angle and ground speed adjustment of aircraft b in the ground inertial reference frame; and (3) the wind speed vector where aircraft b is located is unknown and disturbed, which means that the random crosswind and drift angle should be considered.

The aircraft trajectory measurement is based on discrete sampling using secondary ser radar (SSR) or automatic dependent-broadcast (ADS-B), so the aircraft kinematics equation can be described as a discrete state form $\dot{\boldsymbol{x}}(k) = f(\boldsymbol{u}(k))$, where the position of the aircraft is $\boldsymbol{x}(k) = [x(k), y(k)]^{\mathrm{T}}$, and $\boldsymbol{u}(k) = [v_{GS}(k), \theta(k)]^{\mathrm{T}}$. In the ground inertial reference frame, the two control variants, i.e., the track angle adjustment $\Delta\theta_b$ and the ground speed adjustment $\Delta v_{GS,b}$ of aircraft b are not necessarily zero at the same time, so the trajectory of aircraft b is twisting during conflict resolution, as shown in Fig. 6.

At the beginning of the $k-1$-th receding horizon, if aircraft b deviates from the air route centerline and it is located at position $\boldsymbol{x}_{P1}$, i.e., $\Delta\theta_b(k)\cdot\Delta\theta_b(0) > 0$, and thus the duration of the conflict resolution can be expressed as:

$$\Gamma_3 = \frac{2d_Q\cdot\|\boldsymbol{l}_b\| - |\boldsymbol{l}_b\cdot\boldsymbol{x}_b - c_b|}{\|\boldsymbol{l}_b\|\cdot(v_b+\Delta v_b)\cdot\sin(\Delta\theta_b)}. \tag{13}$$

Else if aircraft b approaches the air route centerline and it is located at position $\boldsymbol{x}_{P2}$, i.e., $\Delta\theta_b(k)\cdot\Delta\theta_b(0)\le 0$, then the duration of conflict resolution can be expressed as:

$$\Gamma_3=\frac{|\boldsymbol{l}_b\cdot\boldsymbol{x}_b-c_b|}{\|\boldsymbol{l}_b\|\cdot(v_b+\Delta v_b)\cdot\sin(\Delta\theta_b)}. \tag{14}$$

When the function of duration is synthesized and expressed in the discrete form, then the optimal conflict resolution for the k-th receding horizon can be expressed as follows:

$$\min J\big(\Delta v_b(k),\Delta\theta_b(k)\big)=\begin{cases}\frac{2d_Q\cdot\|\boldsymbol{l}_b\|-|\boldsymbol{l}_b\cdot\boldsymbol{x}_b(k)-c_b|}{\|\boldsymbol{l}_b\|\cdot(v_b(0)+\Delta v_b(k))\cdot\sin(\Delta\theta_b(k))},\ \Delta\theta_b(k)\cdot\Delta\theta_b(0)>0\\ \frac{|\boldsymbol{l}_b\cdot\boldsymbol{x}_b(k)-c_b|}{\|\boldsymbol{l}_b\|\cdot(v_b(0)+\Delta v_b(k))\cdot\sin(\Delta\theta_b(k))},\ \Delta\theta_b(k)\cdot\Delta\theta_b(0)\le 0,\end{cases} \tag{15}$$

$$\begin{cases}\boldsymbol{x}_a(k)=\boldsymbol{x}_a(k-1)+\dot{\boldsymbol{x}}_a(k)\cdot\Delta\Gamma & \text{(a)}\\ \boldsymbol{x}_b(k)=\boldsymbol{x}_b(k-1)+\dot{\boldsymbol{x}}_b(k)\cdot\Delta\Gamma & \text{(b)}\\ \big|\boldsymbol{l}_b\cdot\boldsymbol{x}_b(k)-c_b\big|-w\cdot\|\boldsymbol{l}_b\|<0 & \text{(c)}\\ \big\|\boldsymbol{x}_r(k)\big\|-d_{\min}>0 & \text{(d)},\end{cases} \tag{16}$$

where $\dot{\boldsymbol{x}}_a(k)=v_{GS,a}\cdot[\cos(\theta_a),\sin(\theta_a)]^{\mathrm{T}}$, $\dot{\boldsymbol{x}}_b(k)=(v_{GS,b}(0)+\Delta v_{GS,b}(k))\cdot[\cos(\theta_b+\Delta\theta_b(k)),\sin(\theta_b+\Delta\theta_b(k))]^{\mathrm{T}}$, and the constraints above are defined as: (a) and (b) are aircraft short term trajectory prediction models, (c) is the border constraint of the air route, and (d) is separation requirement.

An inner-point barrier function can be used to solve the problem of nonlinear optimization with inequalities. The barrier function can be constructed as follows

$$G\big(\Delta v_{GS,b}(k),\Delta\theta_{GS,b}(k),\kappa_1,\kappa_2\big)=J\big(\Delta v_{GS,b}(k),\Delta\theta_b(k)\big)+\sum_{i=1}^{2}\kappa_i\cdot H_i\big(\Delta v_{GS,b}(k),\Delta\theta_b(k)\big), \tag{17}$$

where $\kappa_1,\kappa_2>0$, and $H_i(\Delta v_{GS,b}(k),\Delta\theta_b(k))$ are constructed by inequality constraints (c) and (d) as follows

$$\begin{cases}H_1\big(\Delta v_{GS,b}(k),\Delta\theta_b(k)\big)=\big(w^2\cdot\|\boldsymbol{l}_b\|^2-\big(\boldsymbol{l}_b\cdot\boldsymbol{x}_b(k)-c_b\big)^2\big)^{-1}\\ H_2\big(\Delta v_{GS,b}(k),\Delta\theta_b(k)\big)=\big(\big\|\boldsymbol{x}_r(k)\big\|^2-(d_{\min})^2\big)^{-1}.\end{cases} \tag{18}$$

The descent gradient of the barrier function is respectively calculated as follows

$$\nabla G\big(\Delta v_{GS,b}(k),\Delta\theta_b(k),\kappa_1,\kappa_2\big)=\begin{cases}\frac{\partial J(\Delta v_{GS,b}(k),\Delta\theta_b(k))}{\partial\Delta v_{GS,b}(k)}+\sum_{i=1}^{2}\kappa_i\cdot\frac{\partial H_i(\Delta v_{GS,b}(k),\Delta\theta_b(k))}{\partial\Delta v_{GS,b}(k)}\\ \frac{\partial J(\Delta v_{GS,b}(k),\Delta\theta_b(k))}{\partial\Delta\theta_b(k)}+\sum_{i=1}^{2}\kappa_i\cdot\frac{\partial H_i(\Delta v_b(k),\Delta\theta_b(k))}{\partial\Delta\theta_b(k)}\end{cases} \tag{19}$$

The optimal mixed resolution strategy $\boldsymbol{u}_b^*(k)=[\Delta v_{GS,b}^*(k),\Delta\theta_b^*(k)]^{\mathrm{T}}$ for the k-th receding horizon can be obtained by applying the gradient descent method.

3.2. Wind speed vector identification using ground-based observations

As shown in Fig. 7, we define the wind speed forecasting error vector as $\Delta\boldsymbol{w}^{(P)}=\boldsymbol{w}^{(P)}-\bar{\boldsymbol{w}}^{(P)}$ for position p, where $\boldsymbol{w}^{(P)}$ and $\bar{\boldsymbol{w}}^{(P)}$ represent the actual and forecast wind speed vector respectively, and thus the wind speed vector error field can be defined as a random field $\Delta\boldsymbol{w}:\mathrm{R}^3\to\mathrm{R}^2$, where $\Delta\boldsymbol{w}(p_i)$ represents the wind speed vector error at $p_i(x_i,y_i,z_i)\in\mathrm{R}^3$ [28].

The wind speed vector error field can be treated as a Gaussian with a zero mean value and a covariance matrix of $R(p_i,p_j)\in R^{2\times2}$. If two components of wind speed vector are isotropic, then the covariance matrix can be simplified as:

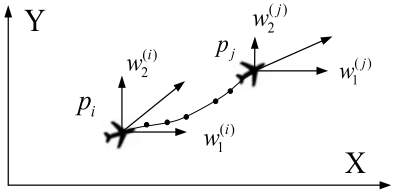

Fig. 7. Wind field along aircraft's trajectory.

$$R(p_i,p_j)=E\big[\Delta\boldsymbol{w}(p_i)\cdot\Delta\boldsymbol{w}^{\mathrm{T}}(p_j)\big]=\begin{bmatrix}r(p_i,p_j)&0\\0&r(p_i,p_j)\end{bmatrix}, \tag{20}$$

where $E[\cdot]$ represents the expected value, and the covariance $r(p_i,p_j)$ can be expressed as:

$$r(p_i,p_j)=\sigma(z_i)\cdot\sigma(z_j)\cdot r_{XY}\big(\|x_i-x_j,y_i-y_j\|\big)\cdot r_Z\big(|z_i-z_j|\big), \tag{21}$$

where $\sigma(z)$ represents the standard deviation of the wind speed error at flight level z. Functions $r_{XY}(\cdot)$ and $r_Z(\cdot)$ both decay exponentially

$$\begin{cases}r_{XY}(s)=c_{XY}+(1-c_{XY})e^{-s/b_{XY}}\\ r_Z(z)=c_Z+(1-c_Z)e^{-z/b_Z},\end{cases} \tag{22}$$

where the values of c_{XY} and b_{XY} were given in [29]. The disturbance of wind speed vector for different waypoints can be simulated using the random wind speed vector error field model described above.

A conflict may not be resolved when the forecast wind speed vector differs greatly from the actual wind speed vector, so the maximum likelihood estimation method and the Newton–Raphson iterative algorithm are employed to identify the actual wind speed vector in an accurate manner.

Let $\boldsymbol{z}_b(k)=[x_b(k),y_b(k)]^{\mathrm{T}}$ be discrete trajectory measurement vector and the sampling interval be $\Delta\tau$. For the reason that $\boldsymbol{z}_b(k)$ might be contaminated by measurement noise, a polynomial smoothing algorithm is employed to pre-processing the noise of trajectory measurement vector series.

Let $\boldsymbol{Z}=[\boldsymbol{z}_b(1),\boldsymbol{z}_b(2),\cdots,\boldsymbol{z}_b(N)]^{\mathrm{T}}$ be the trajectory measurement vector series, the sampling time of $\boldsymbol{z}_b(i)$ be $i\cdot\Delta\tau$, then each discrete trajectory measurement vector can be written by the polynomial:

$$\boldsymbol{z}_b(i)=\boldsymbol{a}_0+\boldsymbol{a}_1(i\cdot\Delta\tau)+\boldsymbol{a}_2(i\cdot\Delta\tau)^2+\cdots+\boldsymbol{a}_p(i\cdot\Delta\tau)^p. \tag{23}$$

Let $\boldsymbol{a}_0'=\boldsymbol{a}_0$, $\boldsymbol{a}_1'=\boldsymbol{a}_1\cdot\Delta\tau$, $\boldsymbol{a}_2'=\boldsymbol{a}_2\cdot\Delta\tau^2$, $\cdots$, $\boldsymbol{a}_p'=\boldsymbol{a}_p\cdot\Delta\tau^p$, and $\boldsymbol{X}=[\boldsymbol{a}_1',\boldsymbol{a}_2',\cdots,\boldsymbol{a}_p']^{\mathrm{T}}$, then the trajectory measurement vector series can be written by:

$$\boldsymbol{Z}=\boldsymbol{H}\cdot\boldsymbol{X}, \tag{24}$$

where

$$\boldsymbol{H}=\begin{bmatrix}1&0&0&\cdots&0\\1&1&1&\cdots&1\\1&1&2^2&\cdots&2^p\\\vdots&\vdots&\vdots&\ddots&\vdots\\1&N&N^2&\cdots&N^p\end{bmatrix}. \tag{25}$$

The unique solution $\hat{\boldsymbol{X}}$ with minimum error is obtained utilizing least square estimation method, then:

$$\hat{\boldsymbol{X}}=\big(\boldsymbol{H}^{\mathrm{T}}\boldsymbol{H}\big)^{-1}\cdot\big(\boldsymbol{H}^{\mathrm{T}}\boldsymbol{Z}\big). \tag{26}$$

Let $\hat{\boldsymbol{Z}}=[\hat{\boldsymbol{z}}_b(1),\hat{\boldsymbol{z}}_b(2),\cdots,\hat{\boldsymbol{z}}_b(N)]^{\mathrm{T}}$ be the estimation of trajectory measurement vector series after polynomial smoothing [30].

$$\hat{\boldsymbol{Z}} = \boldsymbol{H} \cdot \left(\boldsymbol{H}^{\mathrm{T}}\boldsymbol{H}\right)^{-1} \cdot \left(\boldsymbol{H}^{\mathrm{T}}\boldsymbol{Z}\right). \tag{27}$$

Let position $\boldsymbol{x}_b(t)$ be the observation vector, the ground speed $\dot{\boldsymbol{x}}_b(t)$ of aircraft b be the state vector, $\boldsymbol{u}_b(k) = [v_{\mathrm{TAS},b}(k), \varphi_b(k)]^{\mathrm{T}}$ be the input vector, and $\boldsymbol{w} = [w_1, w_2]^{\mathrm{T}}$ be the wind speed vector that needs to be identified. The state and observation equations are expressed as follows:

$$\begin{cases} \dot{\boldsymbol{x}}_b(t) = \left[v_{\mathrm{TAS},b}(k)\cos\varphi_b(k) + w_1,\ v_{\mathrm{TAS},b}(k)\sin\varphi_b(k) + w_2\right]^{\mathrm{T}} \\ \boldsymbol{x}_b(t) = \int_0^t \dot{\boldsymbol{x}}_b(t)dt. \end{cases} \tag{28}$$

The sensitivity equation is obtained by the derivation of $\boldsymbol{w}$ from the observation equation:

$$\frac{\partial \boldsymbol{x}_b(t)}{\partial \boldsymbol{w}} = \begin{bmatrix} t & 0 \\ 0 & t \end{bmatrix}. \tag{29}$$

The objective function of the maximum likelihood estimation can be expressed as:

$$J(\boldsymbol{w}) = \frac{1}{2}\sum_{i=1}^{N}\left[\lambda^{\mathrm{T}}(i)\boldsymbol{R}^{-1}\lambda(i) + \ln|\boldsymbol{R}|\right], \tag{30}$$

where N denotes the sampling number of the measurement vector and input vector, and measurement error is defined as:

$$\lambda(i) = \hat{\boldsymbol{z}}_b(i) - \boldsymbol{x}_b(i). \tag{31}$$

To minimize the objective function $J(\boldsymbol{w})$ by $\boldsymbol{R}$, then

$$\boldsymbol{R} = \frac{1}{N}\sum_{i=1}^{N}\left[\lambda(i)\lambda^{\mathrm{T}}(i)\right]. \tag{32}$$

When the objective function $J(\boldsymbol{w})$ is minimized, the maximum likelihood estimation of the wind speed vector $\hat{\boldsymbol{w}}$ can be obtained [31]. The Newton–Raphson iterative algorithm is usually employed to solve this optimization problem and the iterative equation is:

$$\boldsymbol{w}_{k+1} = \boldsymbol{w}_k + \frac{\sum_{i=1}^{N}[\lambda^{\mathrm{T}}(i)\boldsymbol{R}^{-1}\frac{\partial \boldsymbol{x}_b(i)}{\partial \boldsymbol{w}}]}{\sum_{i=1}^{N}\{[\frac{\partial \boldsymbol{x}_b(i)}{\partial \boldsymbol{w}}]^{\mathrm{T}}\boldsymbol{R}^{-1}\frac{\partial \boldsymbol{x}_b(i)}{\partial \boldsymbol{w}}\}}, \tag{33}$$

where the iteration ends when

$$\left|1 - \frac{J(\boldsymbol{w}_k)}{J(\boldsymbol{w}_{k-1})}\right| \le \varepsilon. \tag{34}$$

3.3. Optimal conflict resolution strategy conversion

After obtaining the maximum likelihood estimation of the wind speed vector $\hat{\boldsymbol{w}} = [\hat{w}_1, \hat{w}_2]^{\mathrm{T}}$ and given the optimal mixed conflict resolution strategy $[\Delta v^*_{\mathrm{GS},b}(k), \Delta\varphi^*_b(k)]^{\mathrm{T}}$ in the ground inertial reference frame, then the track angle and the ground speed of aircraft b for the k-th receding horizon are $\theta^*_b(k) = \theta_b(0) + \Delta\theta^*_b(k)$ and $v^*_{\mathrm{GS},b}(k) = v_{\mathrm{GS},b}(0) + \Delta v^*_{\mathrm{GS},b}(k)$, which can be converted into the optimal onboard aircraft inputs. According to the aircraft speed triangle shown in Fig. 8, the relationship between the true airspeed and the ground speed can be described as follows:

$$\begin{cases} v^*_{\mathrm{GS},b}\cos\left(\theta_b(k)\right) = v^*_{\mathrm{TAS},b}(k)\cos\left(\varphi^*_b(k)\right) + \hat{w}_1 \\ v^*_{\mathrm{GS},b}\sin\left(\theta_b(k)\right) = v^*_{\mathrm{TAS},b}(k)\sin\left(\varphi^*_b(k)\right) + \hat{w}_2 \\ \theta^*_b(k) = \varphi^*_b(k) - \omega_b(k) \end{cases} \tag{35}$$

Thus, the true airspeed and heading angle of aircraft b for the k-th receding horizon is:

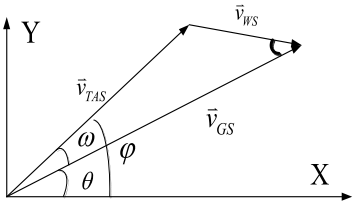

Fig. 8. Aircraft speed triangle.

$$\begin{cases} v^*_{\mathrm{TAS},b}(k) = \left[\left(v^*_{\mathrm{GS},b}\cos\left(\theta^*_b(k)\right) - \hat{w}_1\right)^2 + \left(v^*_{\mathrm{GS},b}\sin\left(\theta^*_b(k)\right) - \hat{w}_2\right)^2\right]^{1/2} \\ \varphi^*_b(k) = \tan^{-1}\left(\left(v^*_{\mathrm{GS},b}\cos\left(\theta^*_b(k)\right) - \hat{w}_1\right) \Big/ \left(v^*_{\mathrm{GS},b}\sin\left(\theta^*_b(k)\right) - \hat{w}_2\right)\right). \end{cases} \tag{36}$$

Thus, the optimal mixed conflict resolution strategy $[\Delta v^*_{\mathrm{GS},b}(k), \Delta\theta^*_b(k)]^{\mathrm{T}}$ for k-th receding horizon, i.e., the ground speed and the track angle of aircraft b are converted into the optimal onboard aircraft inputs $[v^*_{\mathrm{TAS},b}(k), \varphi^*_b(k)]^{\mathrm{T}}$, which ensures that conflicts can be resolved when the forecast wind speed vector differs greatly from the actual wind speed vector.

3.4. Convergence analysis of conflict resolution optimization

Definition 1. For conflict resolution optimization based on RHC, if there are $k_l \in \mathrm{N}$, $k_l < +\infty$ and $\boldsymbol{x}_b(k_l)$ satisfying the following inequality, then the local optimization resolution is achieved.

$$\begin{cases} \boldsymbol{l}_b \cdot \boldsymbol{x}_b(k_l) - c_b < \varepsilon_d \\ \left\|\boldsymbol{x}_r(k_l)\right\| - d_{\min} > 0, \end{cases} \tag{37}$$

where $0 < \varepsilon_d \ll w$ represents allowable deviation from the air route centerline for aircraft b at the end of conflict resolution optimization based on RHC, and Eq. (37) is called local convergence condition.

When aircraft b approaches the air route centerline, i.e., $\Delta\theta_b(k) \cdot \Delta\theta_b(0) \le 0$, for the barrier function shown in Eq. (18) comprises separation factor $\|\boldsymbol{x}_r(k)\|^2 - (d_{\min})^2$, and the objective function shown in Eq. (15) comprises air route deviation factor $|\boldsymbol{l}_b \cdot \boldsymbol{x}_b(k) - c_b|$, after applying the optimal conflict resolution strategy $[\Delta v^*_{\mathrm{GS},b}(k), \Delta\theta^*_b(k)]^{\mathrm{T}}$, there must exist a $k_l \in \mathrm{N}$, $k_l < +\infty$ satisfying $v^*_{\mathrm{GS},b}(k_l) \cdot \sin\theta^*_b(k_l) \cdot \Delta\Gamma < 2\varepsilon_d$.

Suppose that the identification error of wind speed vector is $\boldsymbol{e}_w = [e_1, e_2]^{\mathrm{T}}$, the ground speed error $e_{\mathrm{GS},b}(k_l)$ and the track angle error $e_{\theta,b}(k_l)$ of aircraft b in k_l-th receding horizon can be calculated as follows:

$$\begin{cases} e_{\mathrm{GS},b}(k_l) = \pm\left(e_1^2 + e_2^2\right)^{1/2} \\ e_{\theta,b}(k_l) = \tan^{-1}(e_2/e_1). \end{cases} \tag{38}$$

And the actual ground speed and the actual track angle of aircraft b should be $v^*_{\mathrm{GS},b}(k_l) + e_{\mathrm{GS},b}(k_l)$ and $\theta^*_b(k_l) + e_{\theta,b}(k_l)$, respectively. If the identification error of wind speed vector $\boldsymbol{e}_w$ satisfies the following inequality, then the local optimization resolution is achieved:

$$\left(v^*_{\mathrm{GS},b}(k_l) \pm \left(e_1^2 + e_2^2\right)^{1/2}\right) \cdot \sin\left(\theta^*_b(k_l) + \tan^{-1}(e_2/e_1)\right) < 2\varepsilon_d. \tag{39}$$

Definition 2. For conflict resolution optimization based on RHC, if there are $k_t \in \mathrm{N}$, $k_l \le k_t < +\infty$ and $\boldsymbol{x}_b(k_t)$ satisfying both the local convergence condition and the following inequality, then the global optimization resolution is achieved.

$$\left(\boldsymbol{x}_b(k_t) - \boldsymbol{x}_a(k_t)\right) \cdot \left(\dot{\boldsymbol{x}}_b(0) - \dot{\boldsymbol{x}}_a(0)\right) \ge 0, \tag{40}$$

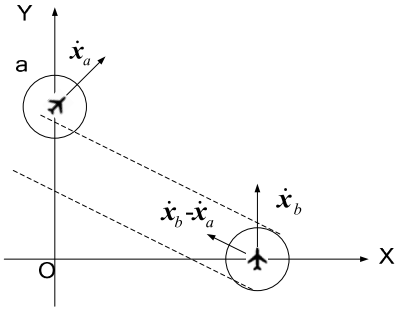

Fig. 9. Initial positions of two aircrafts in the inertial reference frame.

where $\dot{\boldsymbol{x}}_a(0)$ and $\dot{\boldsymbol{x}}_b(0)$ represent the initial ground speed vector of two aircrafts at the beginning of conflict resolution optimization, and Eq. (40) is called global convergence condition.

During conflict resolution optimization, once aircraft b begins to approach the air route centerline, i.e., $\Delta\theta_b(k-1)\cdot\Delta\theta_b(0)>0$, $\Delta\theta_b(k)\cdot\Delta\theta_b(0)\le 0$, the position of aircraft b at the end of conflict resolution optimization based on RHC can be predicted as follows:

$$\frac{\|\boldsymbol{x}_b(k_t)-\boldsymbol{x}_b(k)\|}{v_{\max,b}}\le\frac{\|\boldsymbol{x}_a(k_t)-\boldsymbol{x}_a(k)\|}{v_{\mathrm{GS},a}}\le\frac{\|\boldsymbol{x}_b(k_t)-\boldsymbol{x}_b(k)\|}{v_{\min,b}},\qquad(41)$$

$\boldsymbol{x}_a(k_t)$ and $\boldsymbol{x}_b(k_t)$ satisfy the following air route constraints:

$$\begin{cases}\boldsymbol{x}_a(k_t)\in\{\boldsymbol{x}_a|\boldsymbol{l}_a\cdot\boldsymbol{x}_a(k_t)-c_a=0\wedge(\boldsymbol{x}_a(k_t)-\boldsymbol{x}_a(0))\cdot\dot{\boldsymbol{x}}_a(0)>0\}\\ \boldsymbol{x}_b(k_t)\in\{\boldsymbol{x}_b|\boldsymbol{l}_b\cdot\boldsymbol{x}_b(k_t)-c_b=0\wedge(\boldsymbol{x}_b(k_t)-\boldsymbol{x}_b(0))\cdot\dot{\boldsymbol{x}}_b(0)>0\}\end{cases}\qquad(42)$$

If there exists a solution $\boldsymbol{x}_b(k_t)$ for aircraft b satisfying the global convergence condition at the end of conflict resolution optimization based on RHC, then the conflict resolution strategy in k-th receding horizon is a feasible one. Otherwise, to prevent conflict resolution optimization based on RHC from falling into a local optimum, the following penalty function is added to objective function shown in Eq. (15).

$$P\big(\Delta v_b(k),\Delta\varphi_b(k)\big)=\kappa_3\cdot\max\{0,(\boldsymbol{x}_a(k)-\boldsymbol{x}_b(k))\cdot(\dot{\boldsymbol{x}}_b(0)-\dot{\boldsymbol{x}}_a(0))\}\qquad(43)$$

4. Simulating case study

We consider three cases to verify the effectiveness of the proposed method: static single strategy optimization, dynamic mixed strategy optimization using RHC with one aircraft's ground speed disturbance, and dynamic mixed strategy optimization using RHC with the wind speed vector variation. As shown in Fig. 9, we assume that there are two aircrafts located at the same flight level of 3000 m in the air traffic control area, the initial position of aircraft a is $[0,\ 18\ \mathrm{km}]^{\mathrm{T}}$, the heading angle is $\varphi_a=0.7854$ rad, and the ground speed is $v_{\mathrm{GS},a}=66.7$ m/s, whereas the initial position of aircraft b is $[24\ \mathrm{km},\ 0]^{\mathrm{T}}$, the heading angle is $\varphi_b=1.5708$ rad, and the ground speed is $v_{\mathrm{GS},b}=63.9$ m/s. The distance between aircraft b and aircraft a is $\|\boldsymbol{x}_r\|=30$ km, and the crossing angle is $\beta=1.4289$ rad at present. For the crossing angle $\alpha=1.1268$ rad and $\delta=0.3398$ rad. Apparently, $|\alpha-\beta|<\delta$, and thus there is a potential conflict.

4.1. Static conflict resolution strategy verification

According to the rules of air traffic management, the minimal horizontal separation of the aircraft for radar based air traffic control is $d_{\min}=10$ km and the width of air route is $w=16$ km. In addition, it is assumed that the allowable range of aircraft acceleration a_b is $[-0.61\ \mathrm{m/s^2},0.61\ \mathrm{m/s^2}]$, the allowable range of aircraft ground speed $v_{\mathrm{GS},b}$ is [50 m/s, 83.33 m/s], and the allowable adjustment of heading angle $\Delta\varphi_b$ of aircraft b is less than 0.5236 rad. First, If conflict is resolved by aircraft heading angle adjustment (HAA), then the minimum resolution time $\Gamma_1=412$ s can be obtained when $\Delta\varphi_b=0.2548$ rad and $d_Q=8$ km. However, if the conflict is resolved by the aircraft ground speed adjustment (GSA), then the minimum resolution time $\Gamma_2=529$ s can be obtained when $\Delta v_{\mathrm{GS},b}=-6.08$ m/s and $l_R=35.91$ km. Fig. 10 and Fig. 11 show the trajectories of the two aircrafts during conflict resolution and the curves of the separation between the two aircrafts when static strategies are applied, respectively. It can be concluded that conflict resolution based on the heading angle adjustment is more effective compared with the ground speed adjustment for this case, but the duration of conflict resolution seems too long to be acceptable.

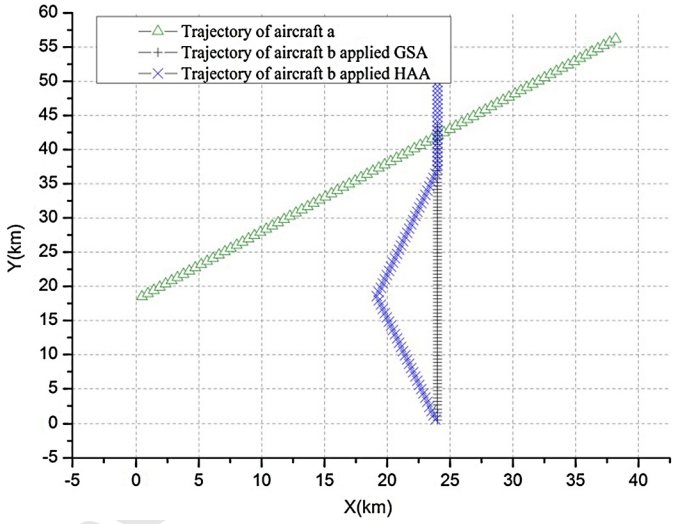

Fig. 10. Trajectories of the two aircrafts when static conflict resolution strategies are applied.

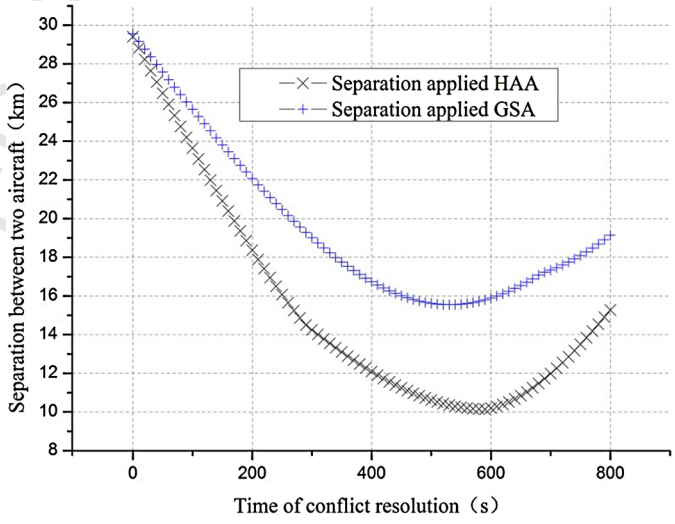

Fig. 11. Curves of the separation between the two aircrafts when static conflict resolution strategies are applied.

4.2. Dynamic conflict resolution strategy verification

We assume that the wind speed vector $\boldsymbol{w}$ remains unchanged and the ground speed of aircraft a begins decelerating to 61.11 m/s

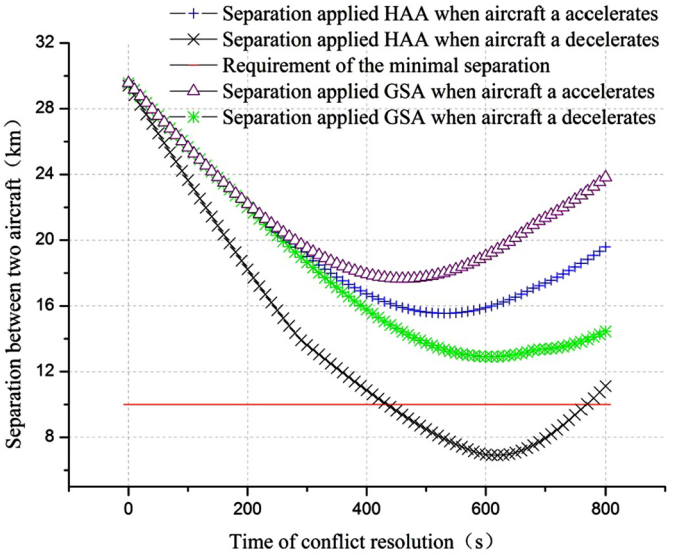

Fig. 12. Curves of the separation between two aircrafts applied previous static strategies.

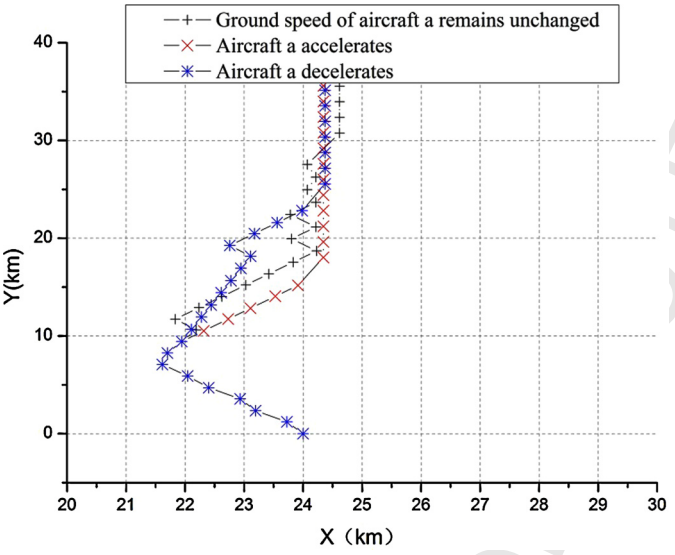

Fig. 13. Trajectories of aircraft *b* when the dynamic resolution strategy is applied with ground speed variation of aircraft *a*.

at -0.61 m/s^2 and accelerating to 72.22 m/s at 0.61 m/s^2 at 30 s after conflict resolution beginning, respectively. If the static conflict resolution strategy is applied before variation of ground speed of aircraft *a*, then the curves of the separation between two aircrafts are shown in Fig. 12. It is obvious that the separation between the two aircrafts cannot meet the requirement of minimal separation if the static heading angle adjustment of aircraft *b* is applied when aircraft *a* decelerates.

However, if we employ the dynamic conflict resolution strategy based on RHC, where we assume that the receding horizon is $\Delta\Gamma = 5$ s, and we set $\kappa_1 = \kappa_2 = 10^{-5}$, then Fig. 13 and Fig. 14 show the trajectories of aircraft *b* when dynamic resolution strategy is applied and the curves of the separation between the two aircrafts with ground speed variation of aircraft *a*, respectively. According to Fig. 14, it only requires 125 s for two aircrafts to resolve conflict when the ground speed of aircraft *a* remains unchanged, but the resolution duration for increases to 135 s when aircraft *a* decelerates to 61.1 m/s at -0.61 m/s^2, whereas the duration reduces to 110 s when aircraft *a* accelerates to 72.2 m/s at 0.61 m/s^2.

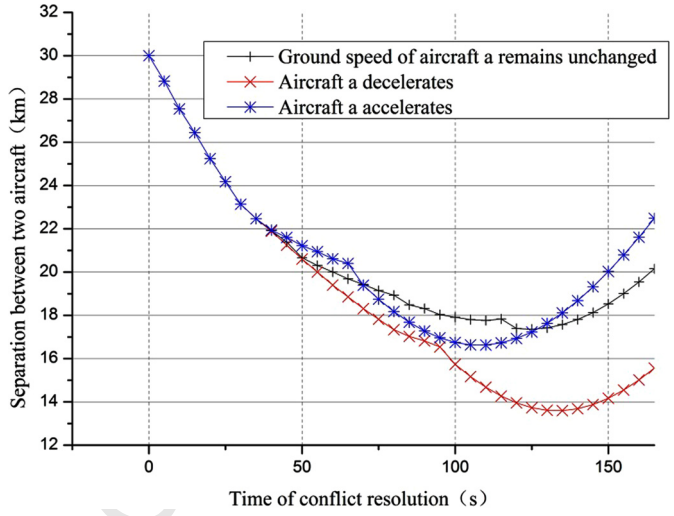

Fig. 14. Curves of the separation between the two aircrafts with ground speed variation of aircraft *a*.

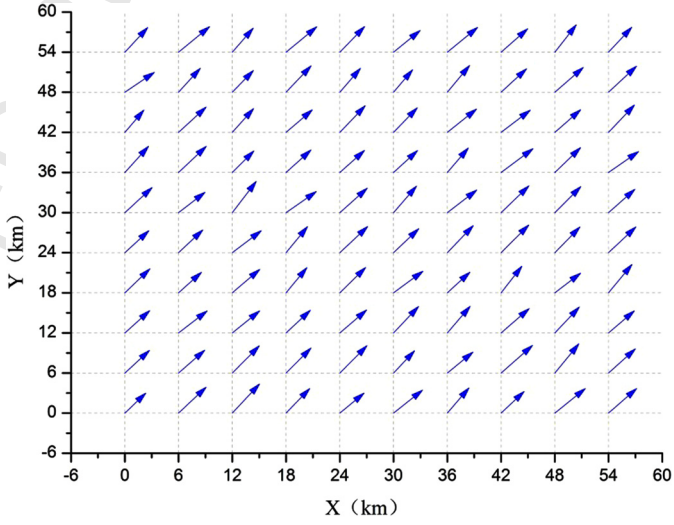

Fig. 15. Random wind speed vector field constructed by the given parameters.

4.3. Wind speed vector identification and conflict resolution verification

Furthermore, let the wind speed vector for the origin of the ground inertial reference frame be $\hat{\boldsymbol{w}} = [7.925 \text{ m/s}, 10.058 \text{ m/s}]^{\mathrm{T}}$. According to [30], for the first component w_1 of the wind speed vector, set $c_{XY} = 0.07$ and $b_{XY} = 231$ km, and for the second component w_2, set $c_{XY} = -0.02$ and $b_{XY} = 241$ km, let $\sigma(z_i) = \sigma(z_j) = 3.9$ m/s and $r_Z(|z_i, z_j|) = 1$ for $z_i = z_j$. We construct a random wind speed vector error using Eq. (20) to Eq. (22), and the generated wind speed vector field within the horizontal area $x, y \leq 60$ km is shown in Fig. 15.

After introducing the wind speed vector field into the aircraft kinematics equation and setting the sampling interval $\Delta\tau$ as 1 s, we can simulate the trajectories of the two aircrafts during conflict resolution, where we acquire 20 samples of true airspeed inputs and trajectory measurements for the two aircrafts before optimizing each conflict resolution strategy. Let the end condition of the Newton–Raphson iterative algorithm be $\varepsilon = 0.001$ in Eq. (34), then the identification of wind speed vector where aircraft *b* is located for each receding horizon is shown in Fig. 16.

The following two situations are considered to compare the impacts on the RHC-based conflict resolution strategy before and after wind speed vector identification, where the first assumes that

Please cite this article in press as: X.-M. Tang et al., Optimal air route flight conflict resolution based on receding horizon control, Aerosp. Sci. Technol. (2016), http://dx.doi.org/10.1016/j.ast.2015.12.024

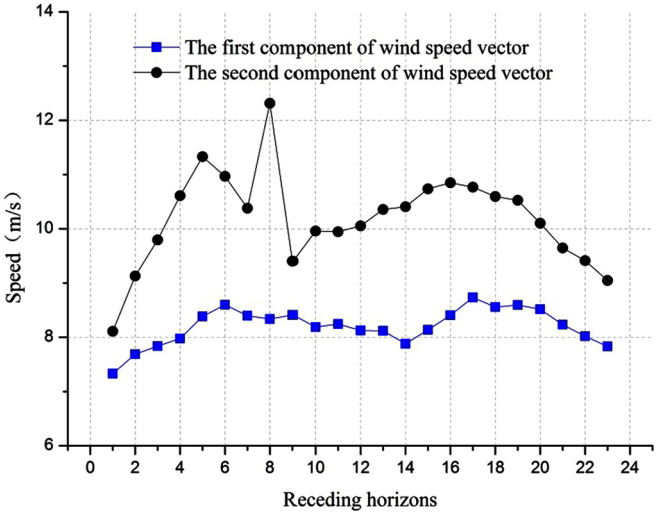

Fig. 16. The identification of wind speed vector for each receding horizon.

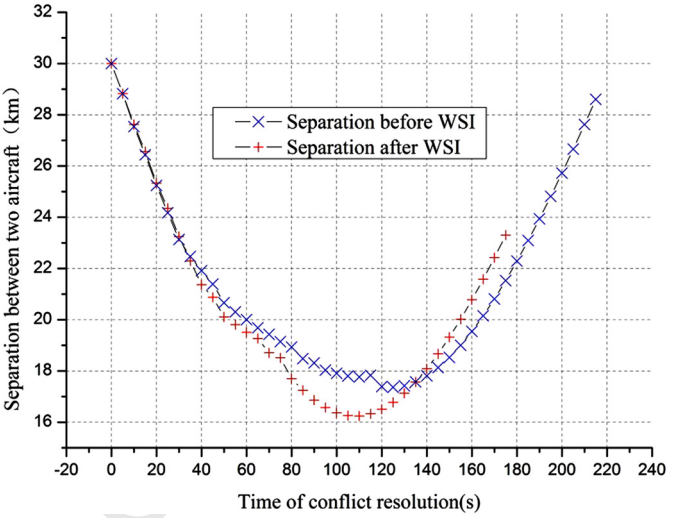

Fig. 18. Curves of the separation between the two aircrafts before and after wind speed vector identification.

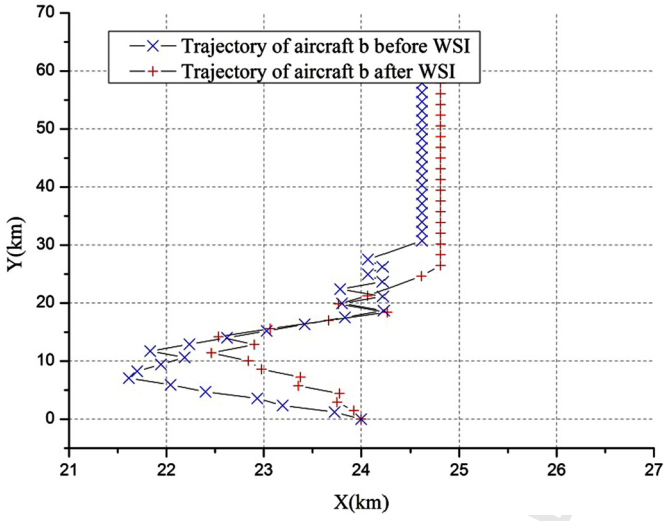

Fig. 17. Trajectories of aircraft b when the dynamic resolution strategy is applied before and after wind speed vector identification.

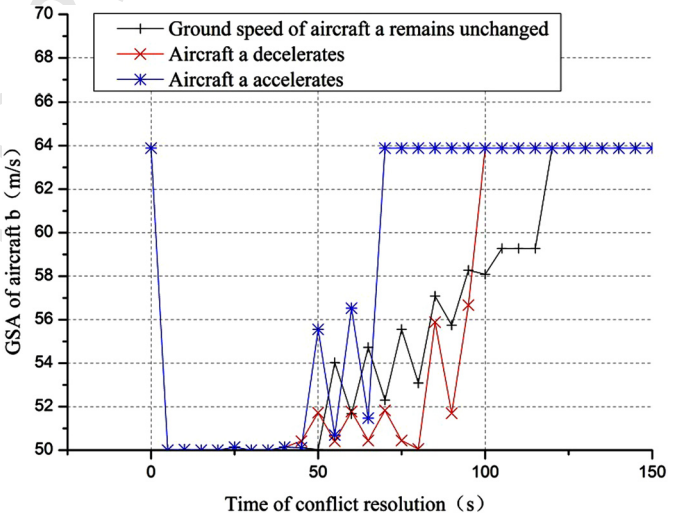

Fig. 19. Ground speed adjustment of aircraft b using dynamic resolution strategy.

wind speed vector identification is not employed and the ground speed $v^*_{GS,b}(k)$ combined with the track angle $\theta^*_b(k)$ is regarded as the input of aircraft b, whereas the second calculates $v^*_{TAS,b}(k)$ and $\varphi^*_b(k)$ using Eq. (36), and the true airspeed $v^*_{TAS,b}(k)$ combined with the heading angle $\varphi^*_b(k)$ are regarded as the inputs of aircraft b. Fig. 17 and Fig. 18 show the trajectories of aircraft b before and after dynamic resolution strategy is applied and the curves of the separation between the two aircrafts before and after wind speed vector identification, respectively. It requires 115 s (i.e., 23 receding horizons) before wind speed vector identification, while it only requires 75 s (i.e., 15 receding horizons) to resolve conflict after wind speed vector identification.

4.4. Analysis of the simulation results

Compared with the static conflict resolution strategy, the duration of conflict resolution is decreased dramatically when a mixed dynamic strategy is applied. Importantly, the minimal separation between two aircrafts is satisfied when aircraft a decelerates and conflict cannot be resolved by static conflict resolution strategy, as shown in Fig. 14. In addition, when the ground speed of aircraft a varies, the dynamic resolution strategy responds to the variation by adjusting the track angle and the ground speed rapidly. As shown in Fig. 19 and Fig. 20, before the ground speed variation of aircraft a, i.e., in the first 6 receding horizons, the ground speed adjustment and track angle adjustment (TAA) remain same for aircraft b, when the ground speed of aircraft a varies in the next receding horizons, the ground speed adjustment and track angle adjustment of aircraft b respond quickly in accordance with the ground speed variation mode of aircraft a, thereby demonstrating the remarkable robustness of the dynamic resolution strategy based on RHC.

The identification error of wind speed vector along the trajectory of aircraft b for each receding horizon is shown in Fig. 21, where the mean absolute errors of the two wind vector components are 0.0136 m/s and −0.0186 m/s, respectively, and the mean relative errors of two wind vector components are 0.173% and −0.205%, respectively.

Next, we should consider the main source of identification error of wind speed vector. We select N samples of true airspeed inputs and trajectory measurements, where the positions of the first sample and the N-th sample are $\boldsymbol{x}_b(k-N)$ and $\boldsymbol{x}_b(k)$, respectively, and the distance from $\boldsymbol{x}_b(k-N)$ to $\boldsymbol{x}_b(k)$ is $d_{k-N,k} = ||\boldsymbol{x}_b(k-N) - \boldsymbol{x}_b(k)||$. Therefore, the wind speed vector error covariance between $\boldsymbol{x}_b(k-N)$ and $\boldsymbol{x}_b(k)$ is $r(\boldsymbol{x}_b(k-N), \boldsymbol{x}_b(k)) = \sigma(z) \cdot r_{XY}(d_{k-N,k})$ according to Eq. (21), and the curve of the covariance with the

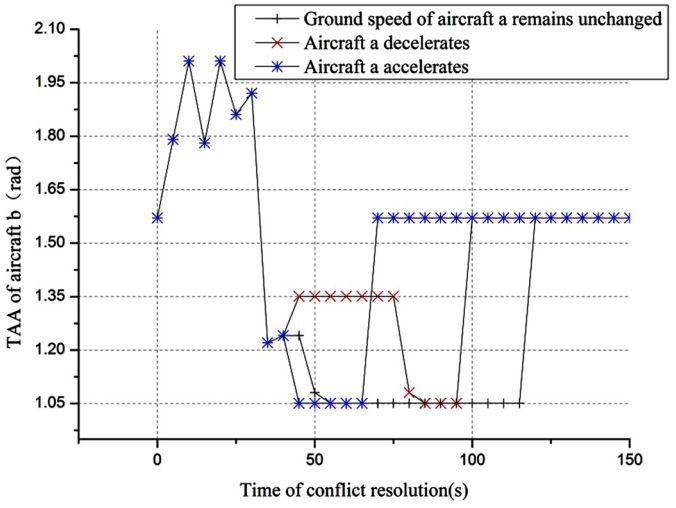

Fig. 20. Track angle adjustment of aircraft *b* in dynamic resolution strategy.

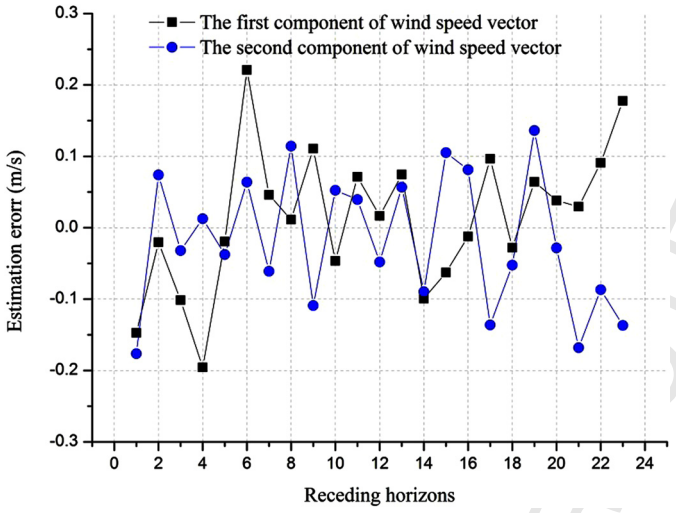

Fig. 21. The identification error of wind speed vector along the trajectory of aircraft *b*.

distance of the two samples is shown in Fig. 22. Obviously, when the distance $d_{k-N,k}$ increases, the wind speed vector error covariance between $\boldsymbol{x}_b(k-N)$ and $\boldsymbol{x}_b(k)$ will decrease, so the wind speed vector identification error increases with number of samples we choose. Thus, to balance the error due to the Newton–Raphson iterative algorithm and the error caused by the samples of true airspeed inputs and trajectory measurements, a reasonable number of samples should be considered for wind speed vector identification.

Compared with the conflict resolution strategy without wind speed vector identification, the duration of conflict resolution is reduced dramatically when using the true airspeed as the input of aircraft *b*. In addition, when the wind speed vector is disturbed, the track angle and the ground speed of aircraft *b* respond effectively to the disturbance via real-time wind speed vector identification. Fig. 23 and Fig. 24 compare the control variants of aircraft *b* before and after wind speed vector identification (WSI), the difference of control variants between the present receding horizon and the last one becomes more distinct, regardless of the track angle and the ground speed, thereby demonstrating the remarkable effectiveness of the dynamic conflict resolution strategy based on RHC while considering wind speed vector identification.

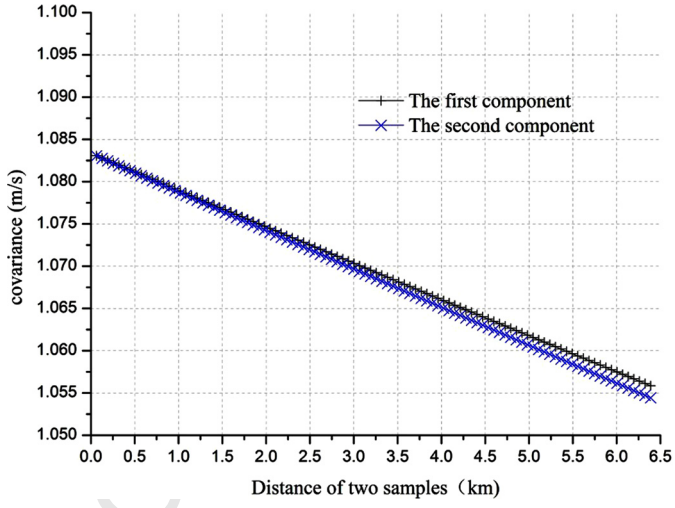

Fig. 22. Curve of the covariance based on the distance between two samples.

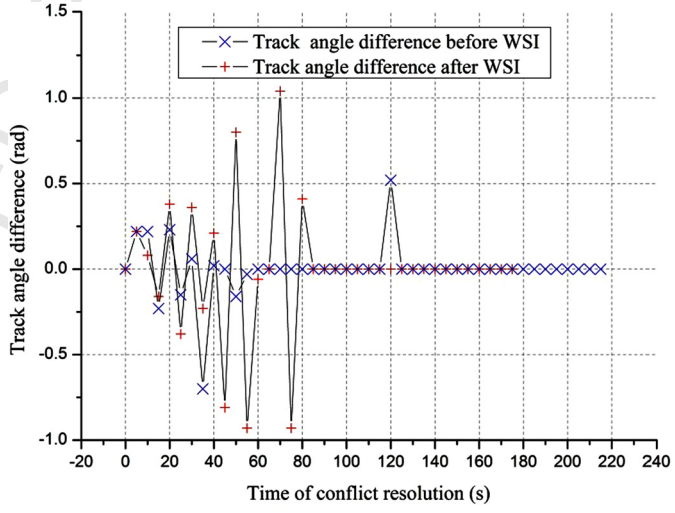

Fig. 23. The difference of track angle between the present receding horizon and the last one.

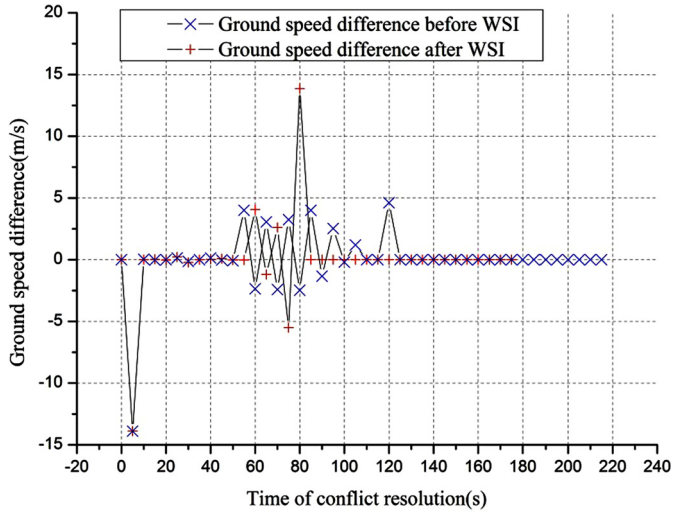

Fig. 24. The difference of ground speed between the present receding horizon and last one.

Please cite this article in press as: X.-M. Tang et al., Optimal air route flight conflict resolution based on receding horizon control, Aerosp. Sci. Technol. (2016), http://dx.doi.org/10.1016/j.ast.2015.12.024

5. Conclusions

In this study, we addressed the problem of dynamic ground conflict resolution for a fix air route. Based on the optimized static single heading or speed adjustment strategy, we proposed an optimized conflict resolution method that uses a dynamic mixed strategy based on RHC. According to our simulation, it requires 125 s for the two aircrafts to resolve conflict when the ground speed of aircraft *a* remains unchanged, the duration of conflict resolution increases to 135 s when aircraft *a* decelerates to 61.1 m/s at -0.61 m/s^2, whereas the duration reduces to 110 s when accelerating to 72.2 m/s at 0.61 m/s^2. Compared with the static conflict resolution strategies, the duration of conflict resolution is reduced dramatically when the mixed dynamic strategy is applied. Importantly, the minimal separation between the two aircrafts is satisfied when aircraft *a* decelerates and conflict cannot be resolved by static conflict resolution strategy, thereby demonstrating the remarkable robustness of the dynamic resolution strategy based on RHC.

In addition, a wind speed disturbance may lead to model mismatching, so we employ the maximum likelihood estimation method and Newton–Raphson iterative algorithm is employed to identify the wind speed vector, and when combined with the aircraft true airspeed inputs and ground based trajectory measurements, the relative identification errors of two wind speed vector components are 0.173% and -0.205%, respectively. According to our analysis, the wind speed vector error covariance between the first and the last sample is negative related to the distance between them, so the wind speed vector identification error will increase if more samples are used. Therefore, to balance the error due to the maximum likelihood estimation method and that caused by the samples of true airspeed inputs and trajectory measurements, a reasonable number of samples should be considered for wind speed vector identification.

According to our simulation, it requires 115 s (i.e., 23 receding horizons) before wind speed vector identification, while it only requires 75 s (i.e., 15 receding horizons) to resolve conflict after wind speed vector identification. Compared with the input of aircraft *b* before and after wind speed vector identification, the difference of the control variants between the present receding horizon with last becomes more distinct, regardless of the track angle and the ground speed, thereby demonstrating the remarkable effectiveness of dynamic conflict resolution strategy based on RHC while considering wind speed vector identification.

However, the application of this method can still be improved in the future if we consider other operational conditions such as the time delay of air ground communication, as well as conflicts with other aircraft in a local conflict resolution optimization.

Conflict of interest statement

None declared.

Acknowledgement

This work was supported by the National Science Foundation of China (61174180), Jiangsu Province Union Innovation Foundation (BY2012014) and by the Chinese Postdoctoral Science Foundation (2014M550291).

Uncited references

[5]

References

[1] H. Erzberger, Automated conflict resolution for air traffic control, in: 25th International Congress of the Aeronautical Science, 2006, pp. 1–27.
[2] C. Tomlin, G.J. Pappas, S. Sastry, Conflict resolution for air traffic management: a study in multiagent hybrid systems, IEEE Trans. Autom. Control 43 (1998) 509–521.
[3] S. Devasia, D. Iamratanakul, G. Chatterji, G. Meyer, Decoupled conflict-resolution procedures for decentralized air traffic control, IEEE Trans. Intell. Transp. Syst. 22 (2011) 422–437.
[4] P.K. Menon, G.D. Sweriduk, Optimal strategies for free-flight air traffic conflict resolution, J. Guid. Control Dyn. 22 (1999) 202–221.
[5] X.M. Jin, S.C. Han, R.F. Sun, Conflict resolution in free flight with linear programming, J. Traffic Transp. Eng. 3 (2003) 75–79.
[6] L.Y. Cheng, S.C. Han, X. Liu, Optical conflict resolution method based on inner-point restriction, J. Traffic Transp. Eng. 5 (2005) 80–84.
[7] A. Valenzuela, D. Rivas, Conflict resolution in converging air traffic using trajectory patterns, J. Guid. Control Dyn. 34 (2011) 1172–1189.
[8] Y.X. Han, X.M. Tang, S.C. Han, Conflict resolution model of optimal flight for fixation airway, J. Traffic Transp. Eng. 12 (2012) 115–120.
[9] J.C. Clements, The optimal control of collision avoidance trajectories in air traffic management, Transp. Res., Part B, Methodol. 33 (1999) 265–280.
[10] X.J. He, Z.W. Liao, Airline flying conflict survey and extrication based on dynamic velocity modulation, J. Comput. Appl. 30 (2010) 540–542.
[11] C. Tomlin, G. Pappas, J. Lygeros, Hybrid control models of next generation air traffic management, in: Lect. Notes Comput. Sci., vol. 1273, 1997, pp. 378–404.
[12] S. Sastry, G. Meyer, C. Tomlin, J. Lygeros, G. Pappas, Hybrid control in air traffic management systems, in: Proceedings of the 34th Conference on Decision and Control, 1995, pp. 1478–1483.
[13] L. Pallottino, E.M. Feron, A. Bicchi, Conflict resolution problems for air traffic management systems solved with mixed integer programming, IEEE Trans. Intell. Transp. Syst. 3 (2002) 3–11.
[14] A. Alonso-Ayuso, L.F. Escudero, F.J. Martin-Campo, A mixed 0–1 nonlinear optimization model and algorithmic approach for the collision avoidance in ATM: velocity changes through a time horizon, Comput. Oper. Res. 39 (2012) 3136–3146.
[15] A. Alonso-Ayuso, L.F. Escudero, F.J. Marin-Campo, A mixed 0–1 nonlinear optimization model and algorithmic approach for the collision avoidance in ATM: velocity changes through a time horizon, Comput. Oper. Res. 39 (2012) 3136–3146.
[16] J. Omer, Comparison of mixed-integer linear models for fuel-optimal air conflict resolution with recovery, IEEE Trans. Intell. Transp. Syst. 16 (2015) 3126–3137.
[17] K. Bilimoria, B. Sridhar, G. Chatterji, Effects of conflict resolution maneuvers and traffic density of free flight, in: Proc. 1996 AIAA Guidance, Navigation, and Control, 1996, pp. 1–11.
[18] A.E. Vela, S. Solak, J.B. Clarke, et al., Near real-time fuel-optimal en route conflict resolution, IEEE Trans. Intell. Transp. Syst. 11 (2010) 826–837.
[19] K. Bousson, Model predictive control approach to global air collision avoidance, Aircr. Eng. Aerosp. Technol. 8 (2008) 605–612.
[20] G.P. Roussos, G. Chaloulos, K.J. Kyriakopoulo, Control of multiple non-holonomic air vehicles under wind uncertainty using model predictive control and decentralized navigation functions, in: Proceedings of the 47th IEEE conference on Decision and Control, 2008, pp. 1225–1230.
[21] G. Chaloulos, P. Hoayem, J. Lygeros, Distributed hierarchical MPC for conflict resolution in air traffic control, in: 2010 America Control Conference, 2010, pp. 3945–3950.
[22] D. Rey, N.E. Faouzi, R. Fondacci, C. Rapine, Assessing the impact of a speed regulation based conflict resolution algorithm on air traffic flow, in: Proceedings of the 5th International Conference on Research in Air Transportation (ICRAT), 2012, pp. 1–8.
[23] C. Peyronne, A. Conn, M. Mongeau, D. Delahaye, Solving air traffic conflict problems via local continuous optimization, Eur. J. Oper. Res. 241 (2015) 502–512.
[24] S. Mondoloni, A multiple-scale model of wind-prediction uncertainty and application to trajectory prediction, in: 6th AIAA Aviation Technology, Integration and Operations Conference (ATIO), 2006, pp. 1–14.
[25] G. Chaloulos, J. Lygeros, Effect of wind correlation on aircraft conflict probability, J. Guid. Control Dyn. 30 (2007) 1742–1752.
[26] Y. Matsuno, T. Tsuchiya, J. Wei, et al., Stochastic optimal control for aircraft conflict resolution under wind uncertainty, Aerosp. Sci. Technol. 43 (2015) 77–88.
[27] D. Delahaye, S. Puechmorel, Aircraft local wind estimation from radar tracker data, in: 10th International Conference on Control, Automation, Robotics and Vision, 2008, pp. 1033–1038.
[28] I. Lymperopoulos, J. Lygeros, Sequential Mote Carlo method for multi-aircraft trajectory prediction in air traffic management, Int. J. Adapt. Control Signal Process. (2010) 830–849.
[29] R.E. Cole, C. Richard, S. Kim, D. Bailey, An assessment of the 60 km rapid update cycle (RUC) with near real-time aircraft reports, 1998, pp. 1–66.

[30] Y.J. Yang, Y.J. Li, J.H. Deng, A new smoother algorithm for pre-processing flight test data, J. Northwestern Polytech. Univ. 16 (1998) 501–505.

[31] Q. Xu, X.M. Tang, S.C. Han, Y.Y. Lu, Short-term 4D trajectory prediction based on parameter identification, Inf. Control 43 (2014) 501–505.